Dynamics modeling of an electro-hydraulically actuated system

Pedro Miranda La Hera
Dept. of Applied Physics and Electronics
Umeå University
xavier.lahera@tfe.umu.se

Abstract *This report presents a discussion of modeling dynamics for the forwarder crane located in our department. To formulate dynamics of this system, standard Euler-Lagrange methods are applied, by considering the crane as a multi-body system composed by links and joints. This leads to a set of differential equations that contain various unknown parameters, which are related to the inertias, masses, and location of center of masses. With the aim of estimating these unknown model parameters, a linear representation of the dynamics equations is derived, in which frictional forces are also included. The parameters are estimated by the use of least-square methods, which is made feasible by the design of optimal periodic trajectories. In the machine, optical encoders and pressure transducers are used for capturing links positions and cylinder forces respectively. The computation of joints torques from cylinder forces is explicitly made by a nonlinear mapping. The results of simulation tests show a significant correspondence between measured and estimated values, validating our modeling approach. In addition, the estimated model parameters are within ranges of physically realizable values.*

1 Introduction

Accurate and fast motions of robot manipulators are today realized by the design of model-based motion control strategies, which employ models of robot kinematics and dynamics. While the kinematics analysis of a serial robotic manipulator concerns mainly positions, velocities and accelerations, the dynamics model is usually understood to be the model relating the generalized forces supplied by its actuators to its motion. From the mathematical point of view, these models form a set of differential equations, which specific solutions describe the overall behavior of the robot. Apart of control design, such models are used in simulation tests for evaluating the performance of different control strategies, and motion planning techniques, prior real time implementation.

The dynamics equations usually contains various parameters categorized as *a*) geometrical, *b*) inertial, and *c*) those used to represent frictional forces. While the geometric parameters are often supplied by the manufacturer of the robot - e.g. in form of standard

engineering drawings - the inertial and frictional parameters are not as readily known. Commonly, rough estimations of the inertial parameters can be drawn from standard CAD models, but due to the complex shapes, and uncertainty in material properties, they tend to be unprecise, and therefore unreliable. A very impractical approach consists of disassembling the robot and performing weighting, balancing, and pendulum tests on each individual link.

Nowadays, the most common approach towards estimation of inertial and frictional parameters is known as robot parameter estimation, or system identification [5]. In this approach we perform data-driven *grey-box modeling* by the use of force-motion data (collected during the execution of a motion), and the equations of motion derived to represent the robot dynamics. In order to apply such an approach, the mathematical relationship in the form of dynamics equations, between the generalized forces, the motion, and the inertial parameters is first required. In addition, measurement devices, such as encoders, accelerometers, force transducers, have to be available for the sensing of the robot and data recording.

Usually, there are ten inertial parameters for each link, i.e. the mass, the three components of the location of the center of mass, and the six components of the inertia tensor. It is been proven that by introducing a suitable transformation, the dynamics equations could be written linearly in terms of a combination of these inertial parameters, see e.g. [7]. With such a representation, techniques developed for least squares methods can be applied to obtain the missing inertial values, provided the trajectory applied is sufficiently exciting to reveal nonlinear dynamic behaviors. However, the accuracy of such estimation is hard to assess, since the values are unknown beforehand.

With this background, lets consider a detailed review of modeling dynamics of a forestry crane, which represents an electro-hydraulically actuated mechanical manipulator.

2 Modeling robot dynamics

2.1 Kinematic modeling

The manipulator used for our study is a downsized version of a typical forwarder crane, but similar in configuration and dynamics (see Fig. 1). It consists of a serial kinematic chain, with a telescopic boom in the end link. The machine uses hydraulic actuation to produce motion at the joint levels. The joints of the robot are structured as follows:

(0) Base of the robot manipulator.

(1) Revolute joint for *slewing*, associated with q_1.

(2) Revolute joint for the *inner boom*, associated with q_2.

(3) Revolute joint for the *outer boom*, associated with q_3.

(4) Prismatic joint for *telescopic extension of the outer boom*, associated with q_4.

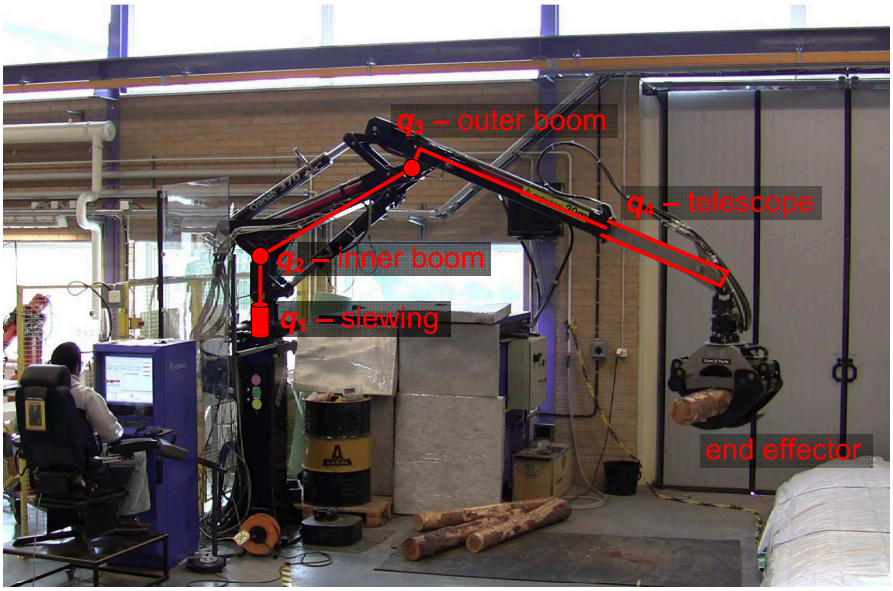

Figure 1: Laboratory crane installed at the Department of Applied Physics and Electronics, Umeå University.

(5) Joint where end effector is attached (*boom tip*).

The joint variables form the vector of generalized coordinates $q = [q_1, q_2, q_3, q_4]^T$, and they are measured by high-resolution encoders. The forward kinematics can be conveniently expressed using the Denavit-Hartenberg (DH) convention [7], where each link configuration is represented by the homogeneous transformation

$$A_i = \mathrm{Rot}_{z,\theta_i}\,\mathrm{Trans}_{z,d_i}\,\mathrm{Trans}_{x,a_i}\,\mathrm{Rot}_{x,\alpha_i}\,, \tag{1}$$

parameterized by joint angle θ_i, link offset d_i, link length a_i, and link twist α_i. Table 1 gives a summary of the geometrical parameters taken from the CAD models provided by the manufacturer of the machine, with the reference frames as shown in Fig. 2.

Table 1: DH parameters

Link i	θ_i [rad]	d_i [m]	a_i [m]	α_i [rad]
1	$q_1(t)$	2.202	0	$\pi/2$
2	$q_2(t) + \theta_{2,0}$	0	1.4	0
3	$\pi/2 + q_3(t) - \theta_{2,0}$	0	0.104	$\pi/2$
4	0	$d_{4,0} + q_4(t)$	0	$-\pi/2$
Constants: $\theta_{2,0} = 0.1192\,\mathrm{rad}$, $d_{4,0} = 1.813\,\mathrm{m}$				

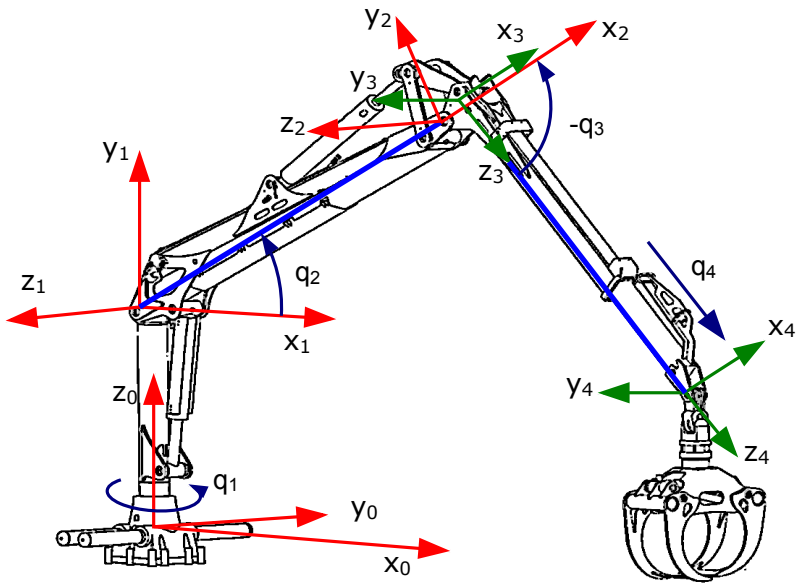

Figure 2: Reference frames to specify the DH convention.

The Cartesian position of the boom tip with respect to the base frame of the robot is defined by

$$p^0 = \begin{bmatrix} x \\ y \\ z \end{bmatrix} = \begin{bmatrix} I_{3\times 3} & 0_{3\times 1} \end{bmatrix} T_4^0 \begin{bmatrix} 0_{3\times 1} \\ 1 \end{bmatrix}, \qquad (2)$$

$$\text{where} \quad T_4^0 = A_1(q_1)A_2(q_2)A_3(q_3)A_4(q_4)\,.$$

2.2 Modeling rigid-body dynamics

Many interesting mathematical models can be created from classical mechanics, when a robot is seen as a system of rigid bodies interconnected by joints, i.e. a multibody system. Classical mechanics has fundamental laws to define how objects move under the action of external forces. The Euler-Lagrange equation is a formalism often used to systematically describe robot dynamics [1, 7, 2, 3]. Below we shall state its main formulation.

For a classical mechanical system, a Lagrangian is the difference of kinetic and potential energy, i.e.

$$\mathcal{L}(q, \dot{q}) = T(q, \dot{q}) - V(q). \qquad (3)$$

For a controlled system with several degrees of freedom (DOF), the Euler-Lagrange equations are given as

$$\frac{d}{dt}\left(\frac{\partial \mathcal{L}(q,\dot{q})}{\partial \dot{q}_i}\right) - \frac{\partial \mathcal{L}(q,\dot{q})}{\partial q_i} = \tau, \qquad i = \{1, 2, \ldots, n\}, \qquad (4)$$

where $q = [q_1, ..., q_n]^T$ are generalized configuration coordinates for the system with n degrees of freedom, $\dot{q} = [\dot{q}_1, ..., \dot{q}_n]^T$ are generalized velocities, and $\tau = [\tau_1, ..., \tau_k]^T$ is the vector of k external forces influencing the systems behavior at the joints level. In a standard mechanical system the kinetic energy is of the form

$$T(q, \dot{q}) = \frac{1}{2}\dot{q}^T M(q)\dot{q}, \tag{5}$$

and the potential energy $V(q)$ is the stored energy that is a function of the systems position. They are usually computed from the homogeneous transformations derived by the kinematic model given in (2), see e.g. [7, 2]. The matrix $M(q)$ is a symmetric and positive-definite matrix of inertias. The controlled Euler Lagrange equation (4) can also be given as a second order differential equation, i.e.

$$M(q)\ddot{q} + C(q, \dot{q})\dot{q} + G(q) = B(q)\tau, \tag{6}$$

where the gravity vector $G(q) = \frac{\partial V(q)}{\partial q}$, and $C(q, \dot{q})$ is the matrix of Coriolis forces.

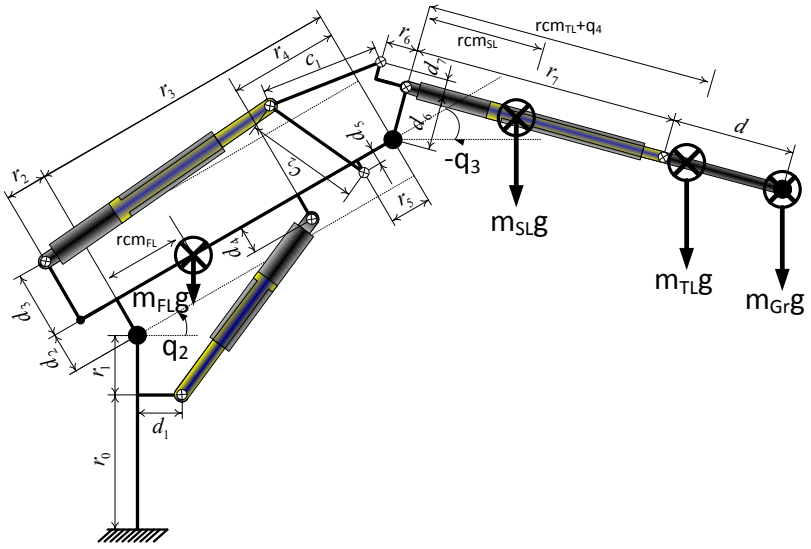

Figure 3: Crane dimensions and masses description in the sagittal plane.

Considering the schematics for the forwarder crane in Fig. 3, the model (6), written for motions in the plane XZ, takes the form

$$M(q_2, q_3, q_4, \xi)\begin{bmatrix} \ddot{q}_2 \\ \ddot{q}_3 \\ \ddot{q}_4 \end{bmatrix} + C(q_2, q_3, q_4, \dot{q}_2, \dot{q}_3, \dot{q}_4, \xi)\begin{bmatrix} \dot{q}_2 \\ \dot{q}_3 \\ \dot{q}_4 \end{bmatrix} + G(q_2, q_3, q_4, \xi) = \begin{bmatrix} \tau_2 \\ \tau_3 \\ F_4 \end{bmatrix}, \tag{7}$$

i.e. the slewing angle q_1 is not considered, and all of the matrices are written in terms of the crane inertial parameters ξ, and the generalized coordinates $q = [q_2, q_3, q_4]^T$. In

addition, and assuming no frictional forces, the set of equations in (7) can be transformed and represented linearly in the elements of the base parameters ξ that constitutes the minimum set, i.e.

$$\varphi(q(t), \dot{q}(t), \ddot{q}(t)) \cdot \theta = \tau, \tag{8}$$

where $\varphi(\cdot)$ denotes the regressor written in terms of the measurable variables $[q, \dot{q}, \ddot{q}]$, θ the minimum set of inertial parameters, i.e.

$$\theta = \begin{bmatrix} m_{FL} \cdot rcm_{FL}^2 + Izz_{FL} \\ rcm_{SL} \cdot m_{SL} \\ m_{SL} \\ m_{Gr} \cdot r_7 + rcm_{TL} \cdot m_{TL} \\ m_{TL} + m_{Gr} \\ m_{Gr} \cdot r_7^2 + m_{TL} \cdot rcm_{TL}^2 + Izz_{SL} + Izz_{TL} + m_{SL} \cdot rcm_{SL}^2 + Izz_{Gr} \\ m_{FL} \cdot rcm_{FL} \end{bmatrix}, \tag{9}$$

and τ the vector of generalized input torques and forces, which is equal to the right hand side of (7).

2.3 Modeling friction forces

Friction forces depend upon the mechanical construction, which include the nature of contact between the parts that produce sliding contact, rolling contact, or a combination of both. In electro-hydraulic servo systems, friction forces are also present at the actuators. The friction is in general velocity dependent and opposite to the motion, but the fluid lubrication, or the solid-to-solid contact of the moving parts dictate, heavily, different regimes of its behavior. In hydraulic manipulators, friction effects are significant, and they constitute a considerable portion of the torque required to drive the links ($\approx 50\%$).

A simple model often used to represent friction considers the static Coulomb - viscous friction, and it is usually formulated as

$$\tau_i^F = f_{c,i} \cdot \mathrm{sgn}(\dot{q}_i) + f_{v,i} \cdot \dot{q}_i, \tag{10}$$

where $i = \{2, 3, 4\}$, and corresponds to the ith link of the robot, f_v denotes the viscous friction, and f_c the coulomb friction. Many real systems exhibit appreciable asymmetric friction forces, i.e. the constant parameters used to represent friction change according to the direction of motion, i.e.

$$f_v = \bar{f}_v + \Delta f_v \cdot \mathrm{sgn}(\dot{q}), \tag{11}$$

$$f_c = \bar{f}_c + \Delta f_c \cdot \mathrm{sgn}(\dot{q}), \tag{12}$$

where the terms with a $\bar{bar}$ denote the mean values, and their variational values Δ depend on the direction of motion given by the $\mathrm{sgn}(\dot{q})$. Introducing the above equations into the general form (10) yields a more suitable model for friction forces, and in the form:

$$\tau_i^F = \bar{f}_{c,i} \cdot \mathrm{sgn}(\dot{q}_i) + \Delta f_{c,i} + \bar{f}_{v,i} \cdot \dot{q}_i + \Delta f_{v,i} \cdot |\dot{q}_i| \,. \tag{13}$$

Despite the simplicity of (13), such model is able to capture the most relevant effects of the nonlinear friction phenomena, and therefore it is widely used for friction estimation.

2.4 Combining the models of dynamics and friction forces

Due to the linearity of the friction parameters in (13), i.e.

$$\tau_i^F = \underbrace{[\text{sgn}(\dot{q}_i) \;\; 1 \;\; \dot{q}_i \;\; |\dot{q}_i|]}_{\varphi_i^f} \cdot \underbrace{\begin{bmatrix} \bar{f}_{c,i} \\ \Delta f_{c,i} \\ \bar{f}_{v,i} \\ \Delta f_{v,i} \end{bmatrix}}_{\theta_i^f}, \tag{14}$$

the introduction of frictional forces into the linear model (8) is straightforward. To show this, we can write a complete set of friction forces for the three links considered, i.e. $q = [q_2, q_3, q_4]^T$, as follows

$$\tau^F = \underbrace{\begin{bmatrix} \varphi_2^f & 0 & 0 \\ 0 & \varphi_3^f & 0 \\ 0 & 0 & \varphi_4^f \end{bmatrix}}_{\varphi^f} \cdot \underbrace{\begin{bmatrix} \theta_2^f \\ \theta_3^f \\ \theta_4^f \end{bmatrix}}_{\theta_f}, \tag{15}$$

where the zero vectors have dimension 1-by-4. Thus, considering that frictions forces act opposed to the torques in the right hand side of (8), a more complete linear model used for parameter estimation is given by

$$[\varphi(q(t), \dot{q}(t), \ddot{q}(t)) \quad \varphi_f(\dot{q}(t))] \cdot \begin{bmatrix} \theta \\ \theta_f \end{bmatrix} = \tau, \tag{16}$$

which results by the combination of (8)-(15), and which does not contradict the linearity property required for system identification.

2.5 Mapping cylinder forces to joint torques

Using the geometry of the machine, the trigonometric mapping between linear cylinder's piston displacement and corresponding joint angle can be found. This mapping $q_i(x_i)$, can be used for *a*) deriving the joint torques, and *b*) computing the velocity of the cylinder's piston given angular velocity.

We begin by considering the virtual work principle [7], to define a relation of the form

$$\tau_i \cdot dq_i = F_i \cdot dx_i, \tag{17}$$

which yields an equality for the joint torque as

$$\tau_i = F_i \cdot \frac{dx_i}{dq_i}, \tag{18}$$

for the links $i = [2, 3]$, as required in (7)[1].

The pressures applied at the chambers of the hydraulic cylinders can be directly measured using pressure transducers. Thus, a direct calculation of the actuators forces can be done considering the schematics in Fig. 4 as

$$F_i = A_{A,i} p_{A,i} - A_{B,i} p_{B,i}, \quad i = \{2, 3, 4\}, \tag{19}$$

where $A_{A,i}$, $A_{B,i}$ denote the areas of chambers A, B respectively, and $p_{(\cdot)}$ the measurements of their corresponding pressures.

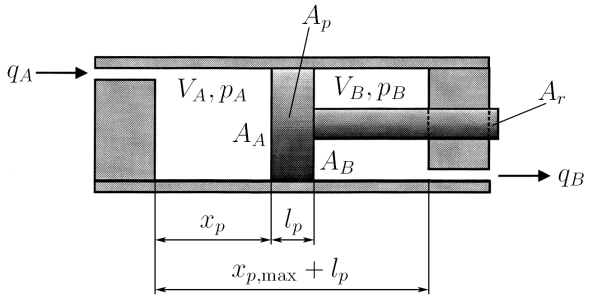

Figure 4: Hydraulic single-rod cylinder [6].

2.5.1 Finding the relation $q_2(x_2)$

In order to calculate the change of linear piston displacement x_2 as a function of the measured joint angle q_2, we apply the following relation

$$x_2(q_2) = \sqrt{j_1^2 + j_2^2 - 2 j_1 j_2 \cos\left(\frac{\pi}{2} - \varphi_4 + \varphi_3 + q_2\right)}, \tag{20}$$

which is derived by the geometry drawn in Fig. 5. In the right hand side of (20), all the parameters are constant (see Fig. 3), with the exception of q_2.

2.5.2 Finding the relation $q_3(x_3)$

The schematics presented in Fig. 6 allow to derive a first set of geometric relations, i.e.

$$\gamma_{21}(q_3) = \frac{\pi}{2} - \beta_1 - q_3 + \gamma_{25}, \tag{21}$$

$$s_{24}(q_3) = \sqrt{s_{22}^2 + s_{23}^2 - 2 s_{22} s_{23} \cos\left(\gamma_{21}(q_3)\right)}, \tag{22}$$

$$\gamma_{24}(q_3) = \arccos\left(\frac{c_1^2 + c_2^2 - s_{24}(q_3)^2}{2 c_1 c_2}\right), \tag{23}$$

which represent the relation of the measured angular motion q_3, with the mechanics driven by the second cylinder. It follows from the schematics in Fig. 7 that the linear

[1]Recall that the telescopic displacement q_4 is linear, and therefore only its cylinder force F_4 is needed in the dynamics (7)

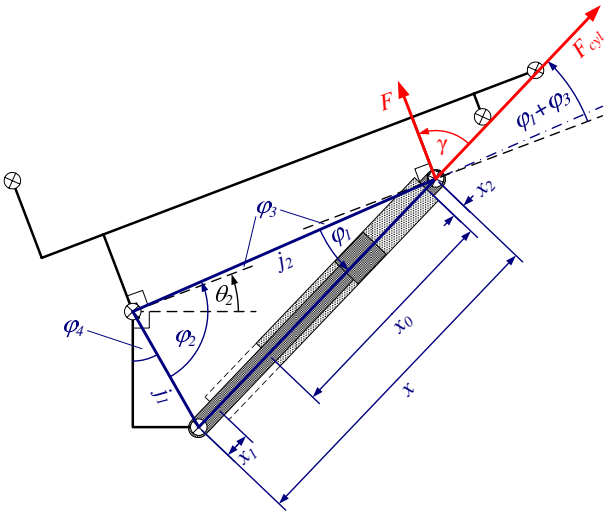

Figure 5: Geometry of the first link.

displacement of the second cylinder can be calculated as

$$x_3(q_3) = \sqrt{s_{33}^2 + s_{31}^2 - 2s_{31}s_{33}\cos(\gamma_{31})}, \tag{24}$$

where the coefficients s_{33} and γ_{31} are functions of q_3. These functions can be computed by the geometrical relations seen from both schematics in Fig. 6-7, and given by

$$\gamma_{31} = \gamma_{21} - \gamma_{32} - \arccos\left(\frac{s_{33}^2 + s_{22}^2 - c_1^2}{2s_{33}s_{22}}\right), \tag{25}$$

$$\gamma_{32} = \arccos\left(\frac{s_{31}^2 + s_{32}^2 - s_{23}^2}{2s_{31}s_{23}}\right). \tag{26}$$

Finally, the vector of generalized forces, in the right hand side of (16), can be computed from (18), (20), (24), as

$$\tau = \begin{bmatrix} \frac{\partial x_2}{\partial q_2} F_2 \\ \frac{\partial x_3}{\partial q_3} F_3 \\ F_4 \end{bmatrix}. \tag{27}$$

3 Estimation of Model Parameters

Recalling that dynamics of the robot can be linearly written in the form

$$\Phi \cdot \Theta = \tau, \tag{28}$$

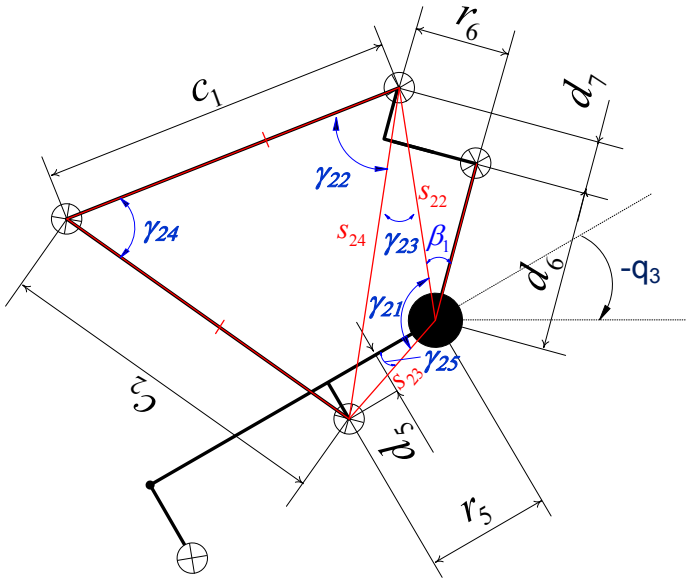

Figure 6: Geometry of the measured angle q_3, with the essential mechanical components that produce its motion.

and that measurements of joint positions and input forces are recorded at each t_i, with $i = \{1, ..., T\}$, an overdetermined matrix of the form

$$\begin{bmatrix} \Phi(t_1) \\ \Phi(t_2) \\ \vdots \\ \Phi(T) \end{bmatrix} \cdot \Theta = \begin{bmatrix} \tau(t_1) \\ \tau(t_2) \\ \vdots \\ \tau(T) \end{bmatrix}, \tag{29}$$

can be formed for finding the values of the vector Θ. The problem with this system is that there is no an unique set of values Θ that satisfy such an equality. It is therefore desired to determine an estimate $\hat{\Theta}$ of Θ that fits the model (29). There are various mathematical forms to define this concept. However, due to its simplicity, the least-square estimate is often used for this purpose.

The least-square estimate is conceptually the value of Θ that minimizes the residual of the vector $|\tau - \Phi\Theta|$. This can be formulated as

$$\min ||\tau - \Phi\Theta||^2 . \tag{30}$$

The least-square estimate can be found as the direct calculation

$$\hat{\Theta} = (\Phi^T \Phi)^{-1} \Phi^T \tau = \Phi^{\dagger} \tau, \tag{31}$$

where $(\Phi^T \Phi)^{-1} \Phi = \Phi^{\dagger}$ is known as the pseudo-inverse of Φ.

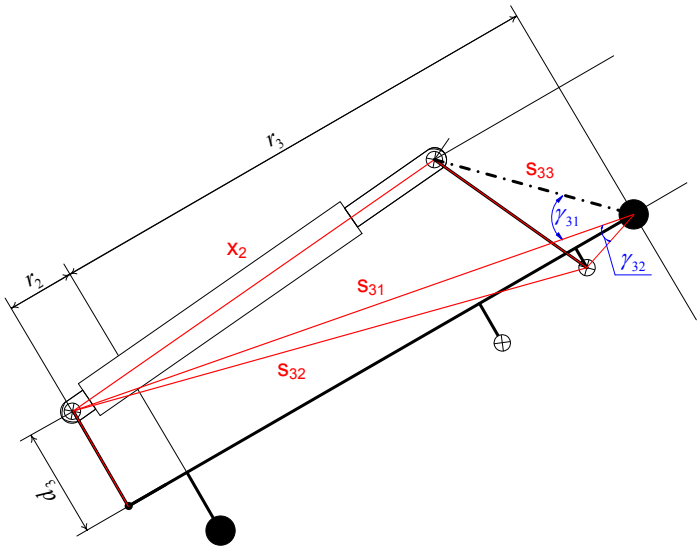

Figure 7: Geometry of the second link cylinder.

3.1 Design of optimal exciting trajectories

The condition number[2] of the matrix Φ can be used as a measure for the sensitivity of the least square solution $\hat{\Theta}$, to perturbations on its elements and τ. Since the elements of $\Phi(q, \dot{q}, \ddot{q})$ are trajectory dependent, we can influence its condition number by designing optimal reference trajectories.

The generation of optimal (or persistently exciting) trajectories has been addressed in several forms. The main difference of approaches is the parametrization used to define the profile of these trajectories. An example is the use of finite Fourier series, yielding a periodic response, i.e. all measured signals are periodic after a transient response. The excitation trajectory for each joint is written as a finite sum of harmonic sine and cosine functions, i.e.

$$q_i(t) = q_{i,0} + \sum_{k=1}^{N} \left[a_{i,k} \sin(k\omega_f t) - b_{i,k} \cos(k\omega_f t) \right], \tag{32}$$

with ω_f being the fundamental frequency of the Fourier series, and which allow to compute the period $T_f = 2\pi/\omega_f$. Each Fourier series contains $2N_i + 1$ parameters, that can be found by optimization. The calculation of the desired joint velocities and

[2]The ration between the maximal and minimal singular values of a matrix. Large condition numbers indicate a nearly singular matrix

accelerations can be performed by analytical differentiation of (32), i.e.

$$\dot{q}_i(t) = \sum_{k=1}^{N} \left[a_{i,k} k\omega_f \cos(k\omega_f t) + b_{i,k} k\omega_f \sin(k\omega_f t) \right], \tag{33}$$

$$\ddot{q}_i(t) = \sum_{k=1}^{N} \left[-a_{i,k} k^2\omega_f^2 \cos(k\omega_f t) + b_{i,k} k^2\omega_f^2 \sin(k\omega_f t) \right]. \tag{34}$$

The choice of the base frequency and the harmonics allows to specify the bandwidth of the excitation signal. Additionally, the use of Fourier series allows continuous differentiation up to any order, which implies the avoidance of unwanted dynamic effects. This global approach to trajectory design allows to excite all joint axes in only one experiment, eliminating the need for special sets of motions.

For our particular purposes, the optimal trajectory was found by optimization techniques designed in the programming environment of MATLAB. The cost function to minimize consists on the condition number of Φ, which value is used to determine the efficiency of the matrix inversion in (31)[3]. The optimization problem is postulated as

$$\min |\text{cond}(\Phi)|, \tag{35}$$

given the constraints on links limits and velocities, as shown in table 2. One of the results of this optimization routine can be seen in Fig. 8, in which the value for the condition number reaches a $\text{cond}(\Phi) = 620$.

Table 2: Position and velocity constraints

Link i	$q_{i,\min}$	$q_{i,\max}$	$\dot{q}_{i,\min}$	$\dot{q}_{i,\max}$
2	-0.45	1.37	-0.16	0.21
3	-2.7	-0.1	-0.43	0.39
4	0	1.55	-0.67	0.5

3.2 Recording data and averaging

In the machine, the exciting trajectories can be realized by decentralized PD feedback gains, i.e.

$$u_i = -K_p(q_i - q_i^{ref}) - K_d(\dot{q}_i - \dot{q}_i^{ref}) + F_f(\dot{q}_i), \tag{36}$$

where K_p denotes the values of proportional gains, K_d the values of derivative gains, and F_f is a term partly used for avoiding dead-zones caused by the hydraulic system. It is worth to mention that the controller is done in the electronic level, which implies that u_i is the input signal to the electro-hydraulic servo valve. This controller is a modified version of [4], and designed for avoiding biased values of the parameters $\hat{\Theta}$ due

[3]Notice that during the optimization routine the ideal derivatives (34) are used for the computation of the regressor $\Phi(q, \dot{q}, \ddot{q})$, and its condition number

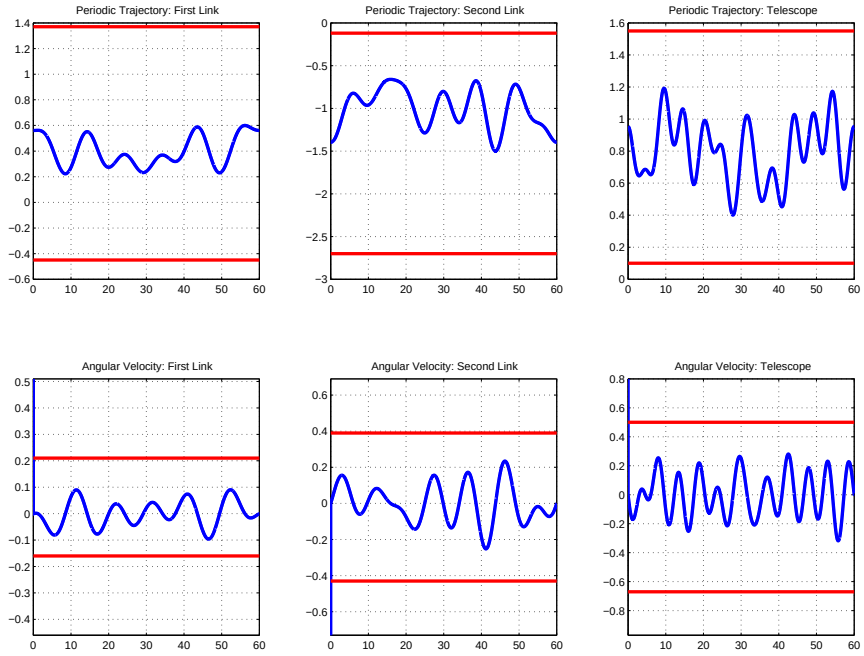

Figure 8: Reference trajectories and velocities for $q = [q_2, q_3, q_4]^T$. The plots also show constraints in positions and velocities.

to feedback [5]. The estimation of velocities and accelerations is done by the use of Kalman filtering.

One advantage of using periodic signals, is the possibility of data averaging. This can be done to improve the signal-to-noise ratio of the measured signals. The averaged trajectory $\bar{q}$ and torque $\bar{\tau}$ are obtained as following:

$$\bar{q} = \frac{1}{M}\sum_{m=1}^{m} q_m \tag{37}$$

$$\bar{\tau} = \frac{1}{M}\sum_{m=1}^{m} \tau_m, \tag{38}$$

with M denoting the number of measured periods, and $()_m$ the measured trajectories and torques. An example of such procedure is shown in Fig. 9, which shows the averaging of one captured data with length 200 seconds (around three periods). The acceleration is estimated off-line from the averaged data set. It can be observed from the recorded torques, that unlike τ_2, i.e. torque in the first link, the nonlinear effects near zero velocity show significant changes for τ_3 and F_4. This is attributed to the friction forces, which for hydraulic systems constitute a considerable portion of the real torque required

to drive the links. Notice that, for example, the forces in F_4 reach magnitudes up to $3000[N]$, when and estimated value of the telescopic link mass with gripper does not exceed $200\,Kg$, i.e. around ten times less force than exhibited by the cylinder.

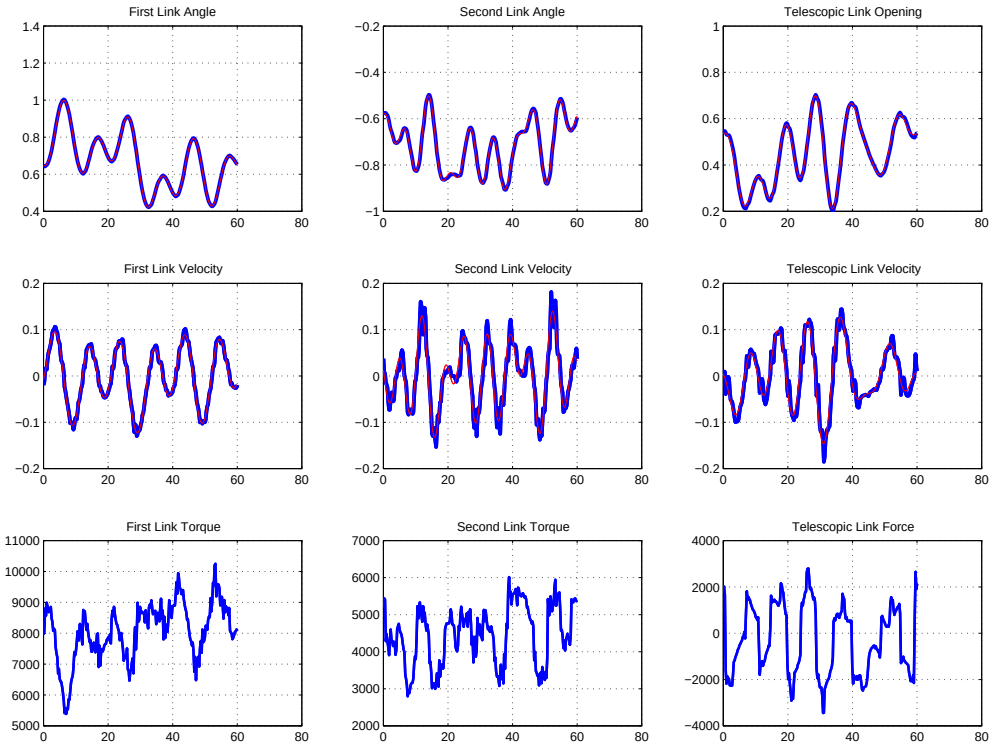

Figure 9: First row: measured trajectories. Second row: measured estimated velocity. Third row: measured torques and forces. The red lines superimposed on the blue lines, represent the reference trajectories and velocities.

3.3 Estimation and validation of parameters $\hat{\Theta}$

A total of 20 different trajectories where recorded to evaluate various ranges of motion. Considering a recursive algorithm of the least-square estimation, a set of parameters $\hat{\Theta}$ was found, within values that are considered physically feasible. Two additional data sets were recorded for validation tests. They are presented in Fig. 10-11, and Fig. 12-13 show the validation tests. The validation shows a comparison of the averaged measured torque $\bar{\tau}_m$, versus the torque computed by the model (16), once the values of the parameters $\hat{\Theta}$ have been estimated. We can see that major dynamics are successfully covered by the model, but unmodeled dynamics are also present.

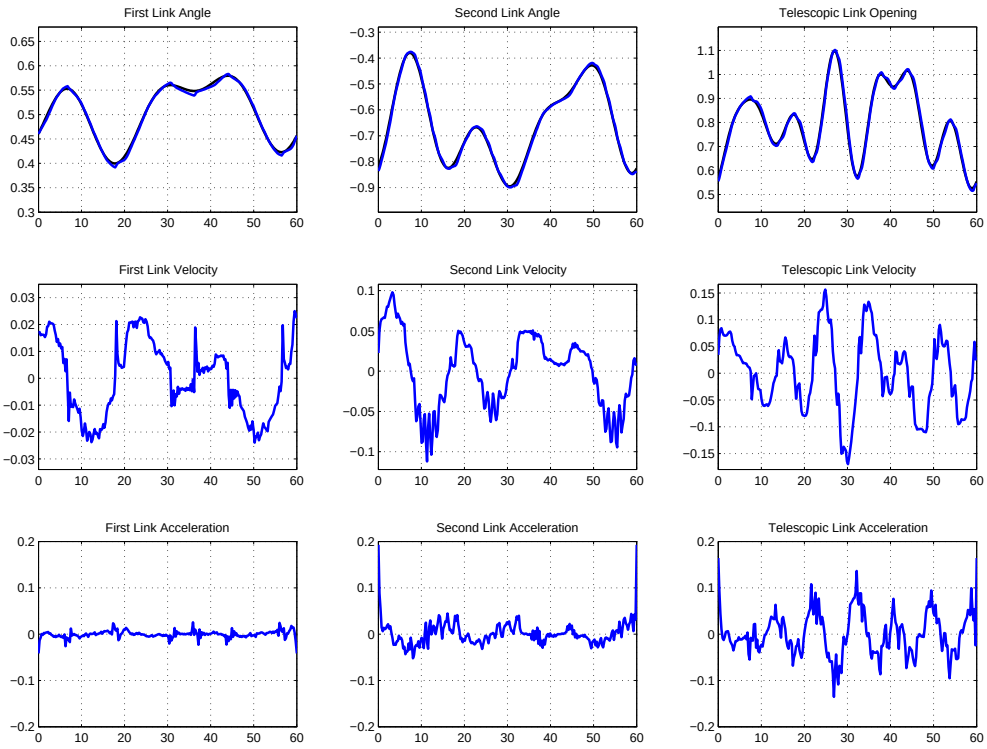

Figure 10: First example of data used for validation. First row: Averaged trajectories. Second row: Averaged velocity. Third row: Estimated acceleration.

4 Concluding remarks

Essential to the design of high performance motion control, is the development of accurate mathematical models describing the robot dynamics. In this project we have dealt with a forestry crane, which consists of an electro-hydraulically actuated robotic manipulator.

A kinematic model was derived to compute the equations of motion that describe the system dynamics. Following advances in robot modeling, we have suggested a transformation of the dynamics equations into a linear form, which is suitable for identifying unknown model parameters. These model parameters represent masses, inertias, and location of center of masses.

To describe the nonlinear frictional forces, a static Coulomb - viscous model was suggested. The coefficients used to describe this model was linearly included in the set of parameters to be estimated.

For the computation of joint torques, from cylinder forces, a geometrical derivation of

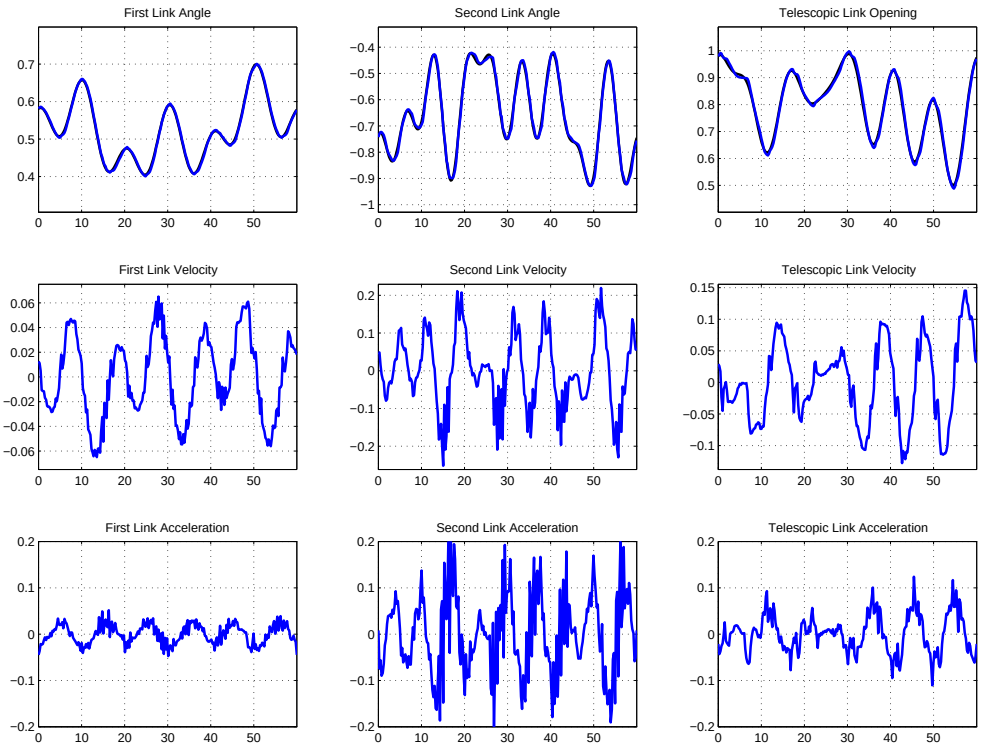

Figure 11: Second example of data used for validation. First row: Averaged trajectories. Second row: Averaged velocity. Third row: Estimated acceleration.

the cylinders displacements as functions of the joint angles was formulated. This allows a direct calculation of the joint torques given measured hydraulic forces.

The technique used for the estimation of missing parameters is based on the least-square method, and its recursive variations. This allows to handle a set of experimental data, rather than single recorded tests. To produce feasible estimates, we design a set of optimal trajectories, where the optimality is referred to the inversion of the systems regressor, and measured by its condition number.

To finalize, we perform various tests, in which different ranges of motions are captured. The physical setup allows to measure links positions, and cylinder forces, and the estimation of velocities and acceleration are done by Kalman filtering. The results allow to assess the correctness of the estimated parameters. We conclude that despite minor differences, the model found is able to capture the most relevant dynamics involved in a motion. Perhaps, additional unmodeled dynamics, which are thought to come from the hydraulic system, could increase the performance of this estimation.

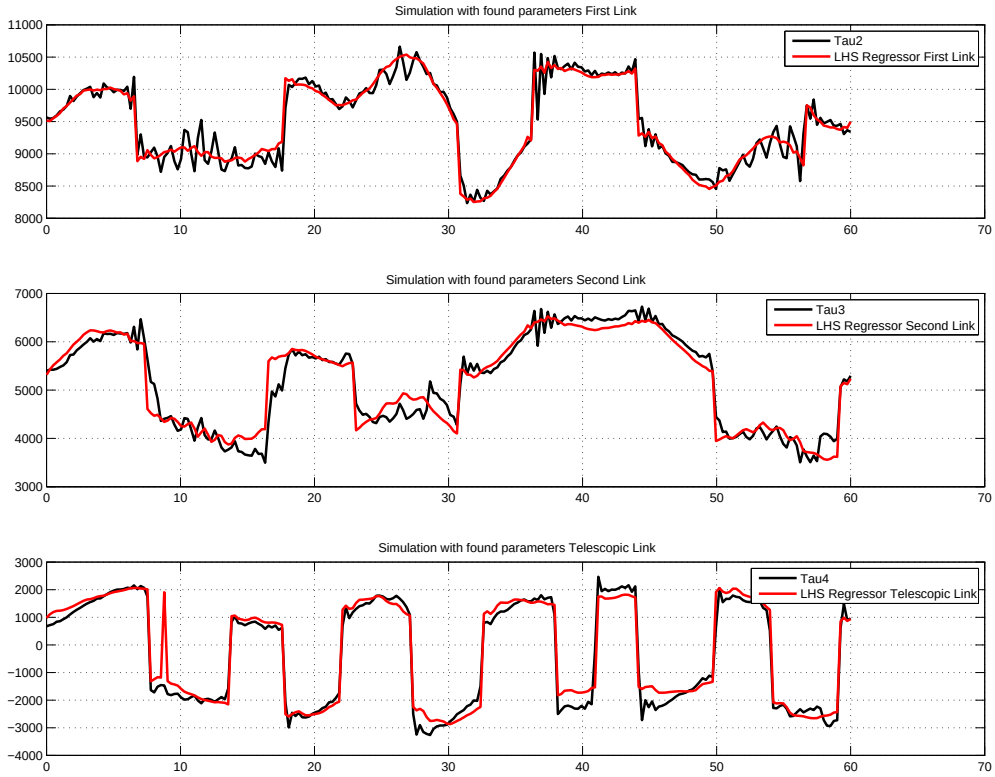

Figure 12: Validation with the first data set from Fig. 10. The plot shows the measured averaged torque (black line) vs. estimated torque (red line).

5 Future plans

The input signal to the forwarder crane corresponds to an electric signal given to the servo valve unit. The task of this valve is to drive the oil to the hydraulic actuators, to produce forces that can induce crane movement. The dynamics of this hydraulic process have not been addressed in this project. Thus, in order to complement the mechanical model developed, we need to formulate the hydraulic dynamics, and run experimental studies to estimate its model parameters, in a similar manner as it was done for the mechanics. Once this full model is developed, we can consider the design of model based control algorithms, with all its possible variations, i.e. computed force control, adaptive control, etc.

Despite the absence of the formulation of hydraulic dynamics, the model presented here can be used in two forms, i.e.

- For observation, which means that it can be used for designing software position

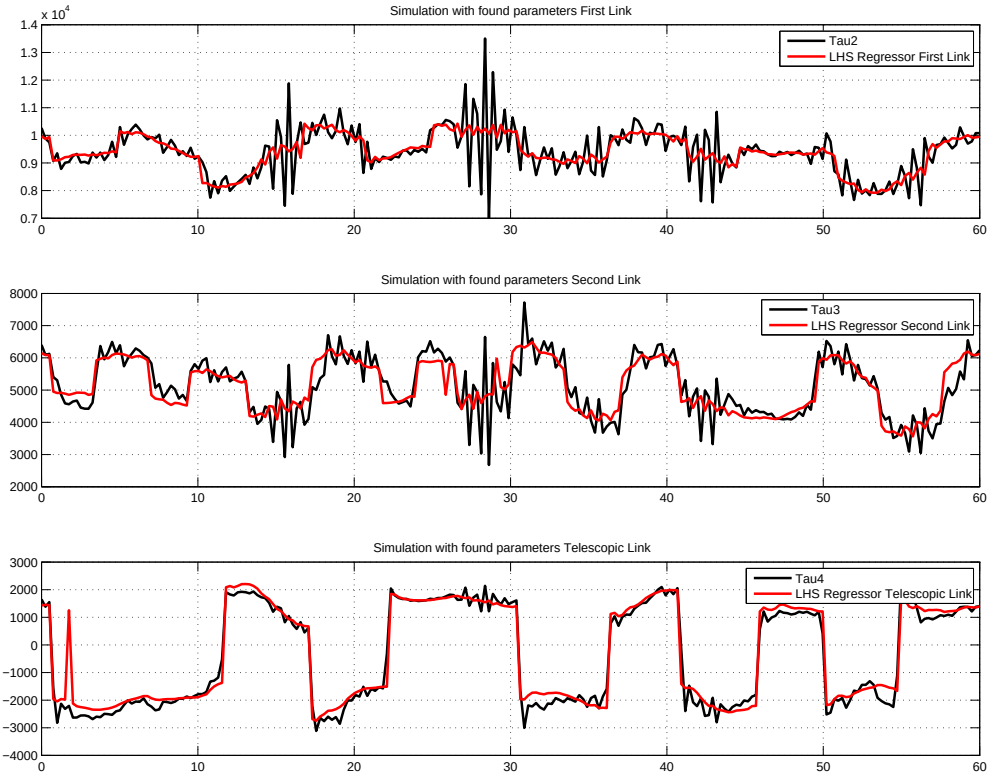

Figure 13: Validation with the second data set from Fig. 11. The plot shows the measured averaged torque (black line) vs. estimated torque (red line).

sensors, for the cases that optical encoders are not available[4]. Additionally, in industry, such models are used for sensor fault detection, which would be of interest for the new cranes designed by Cranab.

- For modeling hydraulic dynamics, which means that this model opens the possibility to apply first principle modeling of the hydraulic components[5].

[4]The availability of pressure measurements opens the possibility to estimate angular position based on model based nonlinear observers

[5]The availability of pressure measurements opens the possibility to understand the complex hydraulic process. Recall that pressure transducers were introduced in 2009, and very few experimental studies were done since then.

References

[1] V. Arnold, *Mathematical Methods of Classical Mechanics (Graduate Texts in Mathematics)*, 2nd ed. New York: Springer, 1989.

[2] J. J. Craig, *Introduction to Robotics: Mechanics and Control*. USA: Prentice Hall, 2003.

[3] L. N. Hand and J. D. Finch, *Analytical mechanics*. USA: Cambridge University Press, 1998.

[4] P. La Hera, U. Mettin, I. Manchester, and A. Shiriaev, "Identification and control of a hydraulic forestry crane," in *Proceedings of the 17th IFAC World Congress*, Seoul, Korea, July 6-11 2008, pp. 2306–2311.

[5] L. Ljung, *System Identification: Theory for the User*. Upper Saddle River: Prentice Hall, 1999.

[6] N. D. Manring, *Hydraulic Control Systems*, 1st ed. New York, USA: John Wiley & Sons, 2005.

[7] M. Spong, S. Hutchinson, and M. Vidyasagar, *Robot Modeling and Control*. New Jersey: John Wiley and Sons, 2006.